



**HAL**  
open science

# Conceptual study of a Compton polarimeter for the upgrade of the SuperKEKB collider with a polarized electron beam

D Charlet, T Ishibashi, A Martens, M Masuzawa, F Mawas, Y Peinaud, D Zhou, F Zomer

► **To cite this version:**

D Charlet, T Ishibashi, A Martens, M Masuzawa, F Mawas, et al.. Conceptual study of a Compton polarimeter for the upgrade of the SuperKEKB collider with a polarized electron beam. *Journal of Instrumentation*, 2023, 18 (10), pp.P10014. 10.1088/1748-0221/18/10/P10014 . hal-04248261

**HAL Id: hal-04248261**

**<https://hal.science/hal-04248261>**

Submitted on 31 Jan 2024

**HAL** is a multi-disciplinary open access archive for the deposit and dissemination of scientific research documents, whether they are published or not. The documents may come from teaching and research institutions in France or abroad, or from public or private research centers.

L'archive ouverte pluridisciplinaire **HAL**, est destinée au dépôt et à la diffusion de documents scientifiques de niveau recherche, publiés ou non, émanant des établissements d'enseignement et de recherche français ou étrangers, des laboratoires publics ou privés.

## 2 **Conceptual study of a Compton polarimeter for the** 3 **upgrade of the SuperKEKB collider with a polarized** 4 **electron beam**

---

5 **D. Charlet,<sup>a</sup> T. Ishibashi,<sup>b</sup> A. Martens,<sup>a,1</sup> M. Masuzawa,<sup>b</sup> F. Mawas,<sup>a</sup> Y. Peinaud,<sup>a</sup>**  
6 **D. Zhou,<sup>b</sup> F. Zomer<sup>a</sup>**

7 <sup>a</sup>*Université Paris-Saclay, CNRS/IN2P3, IJCLab, 91405 Orsay, France*

8 <sup>b</sup>*High Energy Accelerator Research Organization (KEK), Tsukuba 305-0801, Japan*

9 *E-mail: [aurelien.martens@ijclab.in2p3.fr](mailto:aurelien.martens@ijclab.in2p3.fr)*

10 **ABSTRACT:** The physics scope of the Belle II experiment currently acquiring data at the SuperKEKB  
11 collider will expand with a polarized electron beam upgrade, as recently proposed. Among the  
12 required elements for this upgrade, a real time diagnosis of the polarization is necessary to ensure  
13 it is large for all bunches in the accelerator during its regular operation. This will be realized by  
14 inserting a Compton polarimeter in the accelerator. Its conceptual design is described and no show-  
15 stopper for its integration has been identified. An estimation of the sensitivity of the polarimeter  
16 is made by means of toy Monte-Carlo studies. The proposed design accounts for the constraint to  
17 preserve the performance of the SuperKEKB accelerator and to cope with the short time separation  
18 of successive bunches. We show that the polarimeter will measure for each bunch the polarization  
19 within five minutes with a statistical precision below 1% and systematic uncertainties below 0.5%.  
20 It has the capability of providing this information online on a similar timescale. This work paves  
21 the way towards future implementation of real-time Compton polarimetry in several future projects.

22 **KEYWORDS:** Accelerator Subsystems and Technologies; Instrumentation for particle accelerators  
23 and storage rings - high energy (linear accelerators, synchrotrons); Beam-line instrumentation  
24 (beam position and profile monitors, beam-intensity monitors, bunch length monitors)

---

<sup>1</sup>Corresponding author.

---

25 **Contents**

|    |   |           |
|----|---|-----------|
| 26 | <b>1 Introduction</b>                     | <b>1</b>  |
| 27 | <b>2 Compton polarimeter integration</b>  | <b>2</b>  |
| 28 | 2.1 Laser-electron beam interaction point | 4         |
| 29 | 2.2 Photon detector                       | 7         |
| 30 | <b>3 Sensitivity studies</b>              | <b>8</b>  |
| 31 | 3.1 Event generation                      | 9         |
| 32 | 3.2 Fitting procedure                     | 13        |
| 33 | 3.3 Results                               | 16        |
| 34 | <b>4 Summary</b>                          | <b>18</b> |

---

35 **1 Introduction**

36 The Belle II experiment is taking data at the  $e^+e^-$  collision point of SuperKEKB, with a wide  
37 physics program [1]. The collider currently charts new territories in terms of operation luminosity  
38 [2] after having reached a world best in June 2022 [3]. Progress is being made towards reaching  
39 the design luminosity. The very high luminosity reached imposes to refresh the electron bunches  
40 circulating in the SuperKEKB ring regularly by topping up new electrons. This procedure allows  
41 to maintain high beam charge and high luminosity despite slightly perturbing the beam dynamics  
42 [4]. Beyond upgrades of the Belle II detector and interaction point region [5] an upgrade of the  
43 accelerator to allow storage of polarized electrons is being considered [6]. It will extend the physics  
44 scope of the Belle II experiment with unique possibilities to probe the electroweak and dark sectors  
45 and perform unique measurements of Standard Model quantities that are sensitive to new physics  
46 as the tau-lepton anomalous magnetic moment [7].

47 This upgrade involves three main components. Electron beams with high degree of polarization  
48 must be produced and transported to the main SuperKEKB ring. This will be made by means of  
49 strained GaAs lattice illuminated with a circularly polarized laser. A nearly vertical orientation of the  
50 beam polarization is needed for injection in the SuperKEKB ring, in which it will be rotated back and  
51 forth to ensure nearly longitudinal polarization at the Belle II interaction point. This will be made by  
52 means of spin rotators that will be inserted in the ring. This major modification of the SuperKEKB  
53 lattice has been carefully studied keeping in mind the goal of realizing a transparent modification  
54 such that reverting to unpolarized operation of SuperKEKB could be easily done without affecting  
55 accelerator performance. The average polarization of the electrons will be measured over the  
56 lifetime of the accelerator by exploiting the large sample of produced  $e^+e^- \rightarrow \tau^+\tau^-$  events at  
57 Belle II [8]. This measurement will be complemented by an essential, rapid and bunch per bunch  
58 measurement performed by a dedicated Compton polarimeter that will be installed in the ring. This

59 second modification is also required to be transparent for the electron beam. It will be a critical  
60 tool during commissioning and operation to ensure a high beam polarization in the ring. It will  
61 also allow to identify bunches or runs with degraded polarization performance, and thus be used  
62 as an important data quality tool. This polarimeter must thus meet new constraints with respect to  
63 those implemented in the past [9–19] or in other projects [20–23]. In particular, its insertion in the  
64 ring must consist in a minor modification, and in particular we investigate the possibility to insert  
65 the laser system in the SuperKEKB ring itself, without the need for additional excavation. Another  
66 essential aspect is that all bunches are expected to have different polarizations and thus need to be  
67 measured separately typically in timescale corresponding to the refilling of the bunches. This is  
68 also a new requirement to existing polarimeters. For EIC a similar constraint holds [22]. Both of  
69 these aspects are accounted for in the design of the system proposed in this paper.

70 This paper concentrates on the conceptual design and details foreseen performance of the  
71 Compton polarimeter. In section 2, a concept for the integration of the polarimeter is described. In  
72 section 3 a detailed sensitivity study is performed, before one concludes on the remaining works  
73 that need to be done before implementation.

## 74 2 Compton polarimeter integration

75 The SuperKEKB electron-positron collider is currently delivering data to the Belle II experiment  
76 with constantly improving on performances towards design values. It consists of two rings, a high  
77 energy ring (HER) for 7 GeV electrons and a low energy ring (LER) for 4 GeV positrons. The  
78 revolution period is of  $10\mu\text{s}$ . The vacuum of the accelerator and beam induced backgrounds for  
79 the Belle II experiments have been subject to numerous studies [24, 25]. These provide necessary  
80 inputs to the design of the Compton polarimeter for the SuperKEKB polarization upgrade.

81 For this upgrade, spin rotators will be implemented in the SuperKEKB ring upstream and  
82 downstream the interaction point in the HER. These are needed to ensure rotation of the beam  
83 polarization vector from nearly vertical to nearly longitudinal at the Belle II experiment. To this  
84 purpose three different solutions are being considered at this stage. They are summarized here, but  
85 more details are found elsewhere [6].

86 Two of them consist in revisiting the HER lattice over approximately  $\pm 200$  m around the Belle  
87 II interaction point (B2IP), mainly modifying dipole lengths to allow installation of either separated  
88 or combined quadrupole and solenoid magnets. For these two solutions, the spin rotation function  
89 is implemented about 80 meters upstream and downstream B2IP shown in Fig. 1. In this modified  
90 lattice, the region where the beam polarization is nearly longitudinal would be very limited. It  
91 would not leave space to insert a Compton polarimeter to measure a longitudinal beam polarization.  
92 Indeed the straight section of B2IP is already extremely busy and placing a polarimeter in that  
93 region would make it subject to very high backgrounds as radiative Bhabha scattering and beam  
94 induced backgrounds. Further major modification of the lattice would be needed to consider the  
95 implementation of a Compton polarimeter. Alternatively a transverse Compton polarimeter may be  
96 inserted elsewhere in the SuperKEKB ring. This would require a modification of the lattice similar  
97 to that discussed in the rest of the text.

98 The third proposed solution consists in implementing combined function magnets about 210  
99 m upstream B2IP close to the B2E dipoles, see Fig. 1. For this solution, the lattice is minimally

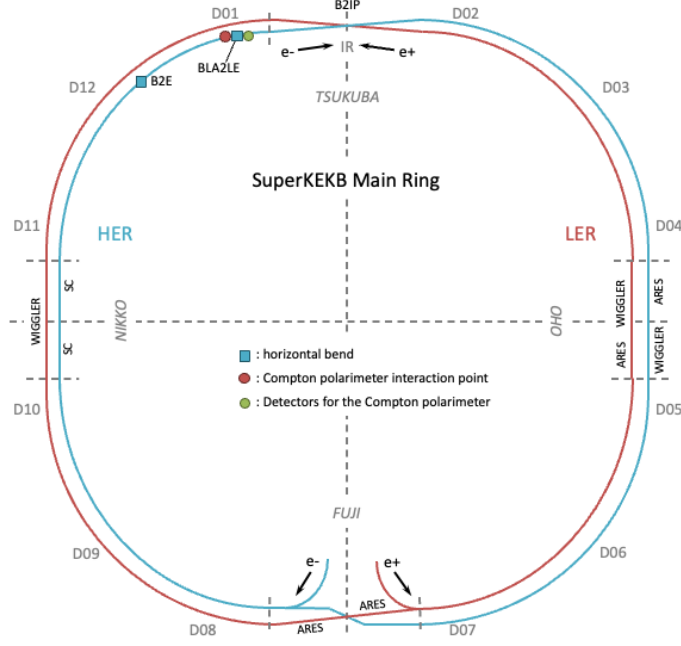


**Figure 1.** Schematic drawing of the main SuperKEKB ring, where the current B2E dipole to be replaced by spin rotators is identified. The location of the Compton polarimeter is also shown as well as Belle II interaction point.

100 modified by replacing the four existing B2E dipoles by newly designed combined function magnets.  
 101 Accelerator tune and chromaticity are matched to that of the current SuperKEKB lattice by adjusting  
 102 strengths of quadrupoles located at a dispersion-free section and retuning sextupoles in arc sections.  
 103 With this proposed solution, it is found that the orientation of the polarization vector is parallel to  
 104 that at B2IP in a region located about 120 to 140 meters upstream B2IP. This part of the lattice  
 105 presents the advantage that there is little existing instrumentation, and thus would facilitate the  
 106 installation of a Compton polarimeter with minimal modification of the existing lattice.

107 The Compton polarimeter consists in a laser system and a detector for scattered particles. The  
 108 laser system and a related vacuum chamber must be inserted in the accelerator tunnel to allow  
 109 interaction of laser and electron beams. The scattered electrons and/or photons must then be  
 110 measured to infer the electron beam polarization. Design and implementation of these detectors  
 111 in the SuperKEKB ring is also an important subject of study. The (Born level) cross-section for  
 112 Compton scattering [26, 27] reads

$$\frac{d\sigma}{dy_c d\phi} = \frac{r_e^2}{x_c} (F_0(r, y_c) + P_L F_L(r, y_c, \phi) + P_C (P_z F_{C,z}(r, y_c) + P_\perp \cos(\phi - \phi_e) F_{C,\perp}(r, y_c))) . \quad (2.1)$$

113 The functions  $F_i$  are given by

$$F_0(r, y_c) = 1 - y_c + \frac{1}{1 - y_c} - 4r(1 - r), \quad (2.2)$$

$$F_L(r, y_c, \phi) = -4r(1 - r) \cos 2(\phi - \phi_L), \quad (2.3)$$

$$F_{C,z}(r, y_c) = y_c \frac{(2 - y_c)(1 - 2r)}{1 - y_c}, \quad (2.4)$$

$$F_{C,\perp}(r, y_c) = -2y_c \sqrt{r(1 - r)}, \quad (2.5)$$

114 where  $y_c = \frac{E_\gamma}{E_e}$  is the ratio of the energy of the scattered photon and the energy of the incoming  
 115 electron,  $r = \frac{y_c}{x_c(1 - y_c)}$ ,  $x_c = \frac{2E_e h \nu_0 (1 + \beta \cos \theta_{\text{in}})}{m_e^2 c^4}$ ,  $\nu_0 = c/\lambda$ ,  $\lambda$  is the laser wavelength,  $h$  the Planck  
 116 constant,  $c$  is the speed of light in vacuum,  $m_e$  is the electron rest mass,  $\pi - \theta_{\text{in}}$  is the crossing angle  
 117 between the two beam directions,  $\beta = \sqrt{1 - 1/\gamma^2}$  with  $\gamma = E_e/m_e c^2$ ,  $\phi$  is the azimuthal angle in  
 118 the observation plane of the scattered photon,  $\phi_L$  is the orientation of the linear polarization of the  
 119 laser beam in the laboratory frame (if any) and  $\phi_e$  is the orientation of the transverse component  
 120 of the electron beam polarization vector with respect to the horizontal direction. The degree of  
 121 linear (circular) laser polarization is denoted by  $P_L$  ( $P_C$ ). The longitudinal and transverse electron  
 122 beam polarization parameters are  $P_z$  and  $P_\perp$ , respectively. For this expression one can draw few  
 123 important remarks when designing a Compton polarimeter. The laser beam polarization needs  
 124 to be circular. Linear laser beam polarization does not contribute to the measurement of the  
 125 electron beam polarization. Inaccuracy in measuring the degree of circular polarization of the laser  
 126 will contribute at the same level to the systematic uncertainties of the electron beam polarization.  
 127 Transverse electron beam polarization can be measured provided that transverse distributions of  
 128 scattered particles are measured, indeed its contribution vanishes after integration over  $\phi$ . On the  
 129 other hand, the longitudinal part of the electron beam polarization can be obtained by measuring  
 130 the energy distribution of the scattered particles. This can be done either by directly measuring  
 131 photons' energies or by measuring position of scattered electrons after a bending magnet. Spatial  
 132 distributions of electrons can thus be measured with pixel detectors to quantify the longitudinal and  
 133 also the transverse component of the electron beam polarization [21, 23]. It is foreseen to implement  
 134 High Voltage – Monolithic Active Pixel Sensors (HVMAPS) for the detection of electrons [6]. In  
 135 this paper we concentrate on the design of a polarimeter based on the detection of photons uniquely,  
 136 that is expected to be less invasive in terms of integration in the existing SuperKEKB ring.

## 137 2.1 Laser-electron beam interaction point

138 The first essential part of the Compton polarimeter consists of a laser system that impinges on the  
 139 electron beam. In order to minimize modifications to the existing infrastructure of SuperKEKB  
 140 and related risks, it is planned to install the laser in the accelerator tunnel rather than excavating  
 141 a new dedicated room. The integrated dose has been measured at the floor of the tunnel in a  
 142 representative area of the accelerator and was measured to be of 0.3mSv/h. This implies a less  
 143 than 1 Gy integrated dose over 6 months of uninterrupted operations of the accelerator. This is  
 144 small with respect to levels that some modern commercial laser systems have been shown to sustain  
 145 [28–30]. Electronics nevertheless require shielding to the neutron flux. This will be made by means  
 146 of Borated Polyethylene walls surrounding electronics boards.

147 The laser will thus be placed on an optical breadboard below the main SuperKEKB ring a  
148 bit upstream from the BLA2LE dipole, where the orientation of the electron beam polarization  
149 is expected to be parallel to that at B2IP, up to residual misalignments [6]. The design of the  
150 vacuum chamber at the Compton interaction point follows several constraints. Crossing angle in  
151 the horizontal plane must be avoided to reduce the effect of synchrotron radiation on the laser  
152 mirrors. A vertical crossing plane is not convenient either for integration purposes. The interaction  
153 chamber is thus designed such that beams cross with some non vanishing azimuthal angle. A first  
154 design of the chamber is shown in Fig. 2. This design exploits the current beam pipe design of  
155 SuperKEKB modified to allow interaction with the laser beam. The effect on the beam impedance  
156 of this modification is found negligible and safe for the electron beam. Projected crossing angles in  
157 the horizontal and vertical planes are about 8 and 4 degrees respectively. It corresponds to a polar  
158 angle of 8.9 degrees and an azimuthal angle of 28 degrees.

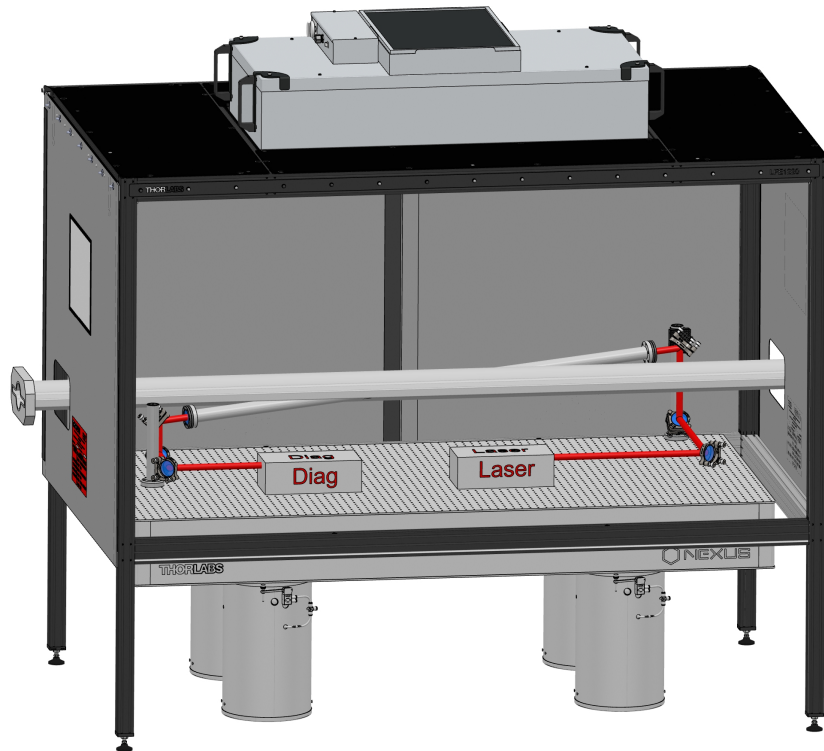


**Figure 2.** Drawing of the laser and electron beams interaction chamber. Boxes named *laser* and *diag* are placeholders for the laser and the diagnostics for the laser light that will be used to ensure that alignment and polarization of the laser are optimized. Not shown are electronics that will be located below the optical table and that will be shielded against the ambient radiation of the accelerator.

159 The laser must comply with the need of colliding bunches at 250 MHz. In the past only CW  
160 or low frequency Q-switched lasers have been implemented in Compton polarimeters [14, 31].  
161 Nowadays the modelock laser technology [32] is very mature and being routinely used, including  
162 in the industry, see for instance Ref. [33] for an overview. This allows to consider the use of an  
163 Ytterbium oscillator locked on the reference frequency of the accelerator. In order to increase the  
164 sensitivity of the Compton polarimeter it is of interest to use second harmonic generation (SHG)

165 to convert infrared light into green light at a wavelength of approximately 515 nm. A telescope is  
166 then employed to adjust the laser beam size, and possibly shape it by means of cylindrical lenses,  
167 so that the luminosity of the interaction is optimized. Continuous measurement of beam position  
168 and pointing will be used in a feedback loop on motorized mounts to ensure a good stability of  
169 the laser beam at the interaction point. The goal being to control this quantity within  $100\mu\text{m}$  and  
170  $100\mu\text{rad}$ . This would ensure a good stability of the luminosity. Polarization independent pickups  
171 will be obtained by means of holographic beam samplers to monitor intensity and polarization  
172 of the beam, that will be adjusted with good quality waveplates. The laser beam will be further  
173 monitored after its interaction with the electron beam to provide further information for calibration.  
174 Absolute calibration of the laser polarization at the interaction point will be made thanks to optical  
175 reversibility [34]. To this end, it is desirable to reflect back a part of the laser light after the  
176 interaction point, and analyze this light [19]. Ideally this mirror must be placed in vacuum. This  
177 would however make maintenance more difficult and is only kept as a backup solution at this stage.  
178 Instead we plan to implement a highly reflective mirror, placed on a motorized mount, right after  
179 the exit window of the vacuum tube. This however does not allow to qualify the laser polarization  
180 at the interaction point but rather after the exit window. Alternatively, anti-reflective coatings can  
181 be used for the optical windows except for the vacuum side of the exit window. In that case most of  
182 the light coming back to the laser from the vacuum chamber would come from the inner side of the  
183 exit window, allowing to indeed calibrate the laser beam polarization at the interaction point. It is  
184 however in practice difficult to implement to ensure a good enough autocollimation. The mirror is  
185 shown on Fig. 3, where the motorized mount is clearly visible. It is interesting to implement this in  
186 any case for alignment purposes by means of autocollimation.

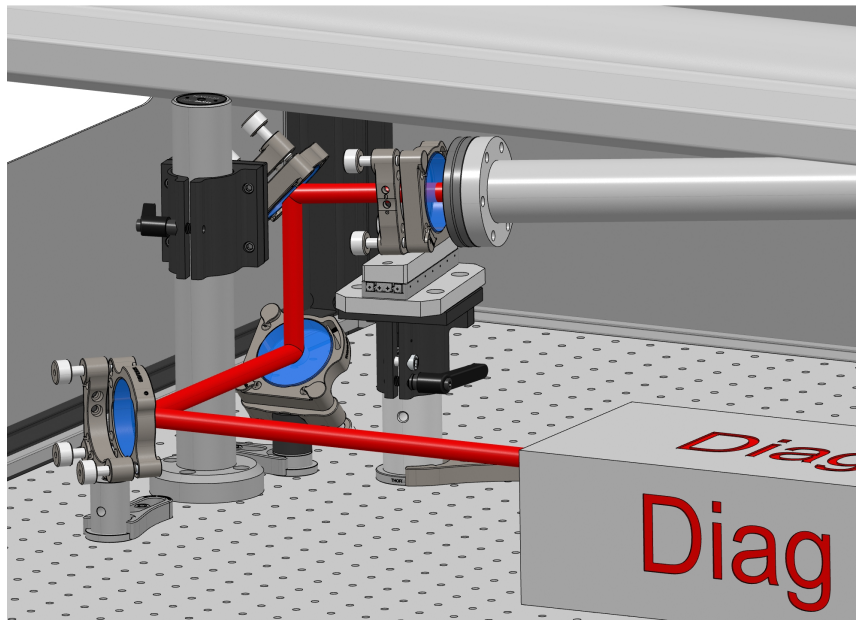


**Figure 3.** Drawing of the insertable mirror after the exit mirror that can be used for calibration of the laser polarization.

## 187 2.2 Photon detector

188 The photon detector aims at distinguishing photons backscattered off electrons from successive  
189 bunches, that are separated by 4 ns. Indeed, due to the top-up injection of SuperKEKB, the  
190 polarization level is expected to vary bunch per bunch. In practice it may even be beneficial to inject  
191 and store beams with opposite polarizations to allow canceling systematic uncertainties related to  
192 time varying detector efficiencies. Assuming that a single photon is impinging the detector at every  
193 bunch crossing, a yearly energy deposited by the signal of 0.4 MJ in a scintillation calorimeter is  
194 anticipated. It corresponds to a 0.2 MGy dose if this energy is supposed homogeneously distributed  
195 over a crystal of  $5 \times 5 \times 25\text{cm}^3$  size. This large dose accompanied with the short time separation of  
196 incoming photons suggests to employ a radiation tolerant scintillation crystal with a fast fluorescence.  
197 Crystals made of BaF<sub>2</sub> are well suited, provided that their intrinsic slow component is reduced by  
198 Yttrium doping and/or the use of solar blind photodetectors [35]. If some studies have already been  
199 made for such a type of detector in the past in the context of Mu2e, a specific work is required for the  
200 purpose of the SuperKEKB Compton polarimeter. The minimal length of the BaF<sub>2</sub> crystal has been  
201 estimated to be 25 cm (approximately 12 radiation lengths) to maintain the mean energy leakage  
202 below 10% for 1.5 GeV photons. It has been estimated using the mean longitudinal profile of the  
203 energy deposition in an electromagnetic cascade initiated by photons [36]. With such a length,  
204 leakage will be dominated by the transverse development of the electromagnetic shower. The final  
205 choice of the transverse size and shape of the crystal will be confirmed at a later stage of the design,  
206 based on detailed GEANT4 simulations. The readout of the scintillation light will be done thanks  
207 to a photomultiplier (PMT), the choice of which will be carefully made to preserve the temporal  
208 profile of the signal impulse. This PMT may either be placed on the ground, about one meter below  
209 the scintillation crystal by guiding the light from the crystal output to the PMT photocathode or  
210 right after the crystal with a short light guide. It will be decided at a later stage of the design based  
211 on induced energy and temporal spreads due to the light guiding. Presence of residual fringe fields  
212 from close-by magnetic elements of the SuperKEKB lattice and radiations at the beam level may  
213 require an additional careful shielding of the detector. Readout electronics will be located nearby  
214 on the ground. The analog part of the acquisition chain will be carefully studied and the signals  
215 will be treated, after digitization, by means of a FPGA (Field Programmable Gate Array) to fill  
216 histograms in for every bunch at 250 MHz. The detailed design of the detector and readout will be  
217 realized in the coming years based on experimental results obtained with a prototype detector.

218 The produced photon beam goes through the BLA2LE dipole without hitting the beam pipe,  
219 providing that the pumping ports integrated in the pipe structure are put on the other side. This  
220 modification is feasible and mainly consists in producing new vacuum pipes. The photon beam also  
221 goes through a quadrupolar magnet and a vertical beam position monitor without interacting with  
222 these elements. The vacuum pipe is then modified to integrate the detector. These modifications are  
223 drawn in Figure 4 where the detector is shown in green. A violet tube of diameter 6mm representing  
224 the photon beam is shown. It roughly corresponds to an emission cone of  $\pm 3/\gamma$ . The involved  
225 modification is not affecting the electron beam impedance, and thus acceptable with that respect.

The detector must be shielded against the synchrotron radiation generated by this deflecting  
dipolar field. For a given deflection angle of  $\theta_B = 20$  mrad, the magnetic field of the magnet  
amounts to 79 mT approximately for a length of  $L_B = 5.9$  m. The critical energy of the synchrotron

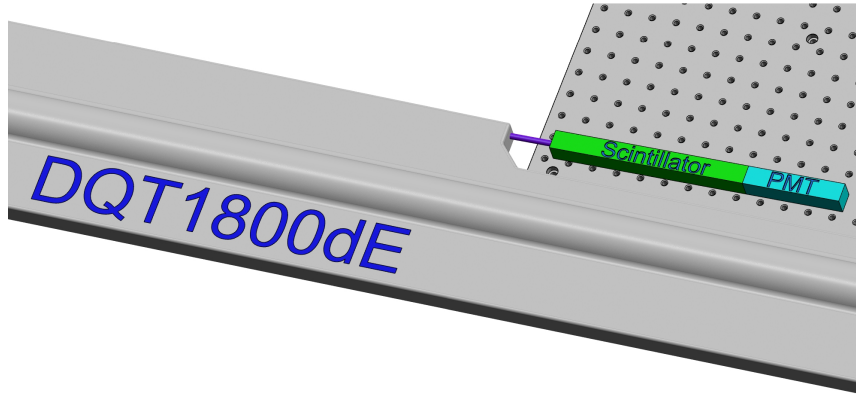


**Figure 4.** Drawing of the modified beam pipe for the insertion of the photon calorimeter in the SuperKEKB ring.

energy spectrum reads [37]

$$E_c = \frac{3}{2} \gamma^3 \frac{\hbar c \theta_B}{L_B} \approx 2.7 \text{ keV}.$$

226 Placing a 4 mm thickness Copper window in front of the detector will cut-off most of the photons  
 227 emitted by synchrotron radiation. The average number of photons impinging the detector amounts  
 228 to 0.06 per 10 nC electron bunch crossing at the Compton IP, corresponding to a 3 keV average  
 229 deposited energy in the calorimeter. Using a 2 mm thickness instead would induce a deposit  
 230 of approximately 300 keV corresponding to approximately six photons per bunch per revolution.  
 231 Compton backscattered photons will also interact in this window, inducing mainly a smearing of  
 232 the energy and angular distributions and  $e^+e^-$  pairs production. Mean energy loss for photons of  
 233 more than 100 MeV is estimated to be below 1% for a 4 mm Cu thickness. Note that the current  
 234 thickness of the SuperKEKB beam pipe is of 6 mm. A detailed study of this effect by means of  
 235 GEANT4 simulations is beyond the scope of this paper and will be performed at the next stage of  
 236 the project. It will be used to decide on the final metallic window type and thickness. The detector  
 237 energy resolution will depend on several parameters as the light yield, the performance of the  
 238 electronics, the fluctuation of the energy leakages (transverse and longitudinal) and the fluctuation  
 239 of the energy pedestal. These detailed studies are outside the scope of this paper but are the core  
 240 subject of the next stage of the development of the polarimeter. In order to assess the performance  
 241 of the detector we will employ crude simplifying assumptions, only providing an estimate for the  
 242 detector resolution.

### 243 3 Sensitivity studies

244 We have developed a standalone generator and fitter for the purpose of validating the proposed  
 245 concept on rapid simulations. Further detailed GEANT4 simulations will be performed at a later  
 246 stage of the design. At this stage of the design, the goal is to validate the fitting procedure on this  
 247 rapid and simplified simulation and realize a preliminary assessment of systematic uncertainties.

### 248 3.1 Event generation

249 The event generation is composed of few ingredients. First electrons are sampled according to the  
 250 electron beam phase space at the expected Compton IP obtained from up-to-date detailed simulations  
 251 of the accelerator. Second the Compton cross-section is implemented. Thirdly backgrounds are  
 252 modeled and implemented in the simulation. Finally interaction in the detector is modeled.

253 Simulated electrons are randomly generated using Eqs. 3.1 where one implicitly assumes that  
 254 the Compton IP longitudinal extension is small with respect to the distance of which the electron  
 255 beam parameters significantly vary [38, 39]. It allows to consider constant beam parameters in the  
 256 interaction region.

$$x_e = \sqrt{2u_x \epsilon_x \beta_x} \cos \phi_x + \eta_x \delta \quad (3.1)$$

$$y_e = \sqrt{2u_y \epsilon_y \beta_y} \cos \phi_y + \eta_y \delta \quad (3.2)$$

$$x'_e = -\sqrt{2u_x \frac{\epsilon_x}{\beta_x}} (\alpha_x \cos \phi_x + \sin \phi_x) + \eta'_x \delta \quad (3.3)$$

$$y'_e = -\sqrt{2u_y \frac{\epsilon_y}{\beta_y}} (\alpha_y \cos \phi_y + \sin \phi_y) + \eta'_y \delta \quad (3.4)$$

257 where  $u_{x,y}$ ,  $\phi_{x,y}$  and  $\delta$  are random numbers with probability density functions given by an expo-  
 258 nential  $\exp(-u)$ , a uniform function in the range  $[0, 2\pi]$  and a Gaussian distribution  $\exp\left(-\frac{\delta^2}{2\sigma_\delta^2}\right)$ ,  
 259 respectively. The Twiss parameters of the beam are represented by  $\alpha_{x,y}$  and  $\beta_{x,y}$ , the RMS emit-  
 260 tance by  $\epsilon_{x,y}$  and the dispersion parameters  $\eta_{x,y}$  and  $\eta'_{x,y}$ . The parameter  $\sigma_\delta = \frac{\sigma_E}{\mu_E}$  is related to  
 261 the energy spread of the electron beam  $\sigma_E$  and its mean energy  $\mu_E$ . The electron beam parameters  
 262 used in the simulation are summarized in Table 1.

**Table 1.** Table of nominal electron beam parameters used for the simulation.

| Parameter        | Value                       |                             |
|------------------|-----------------------------|-----------------------------|
| $\mu_E$          | 7 GeV                       |                             |
| $\sigma_\delta$  | $6.3 \times 10^{-4}$        |                             |
| $Q_e$            | 10 nC                       |                             |
| $T_{\text{rev}}$ | 10 $\mu$ s                  |                             |
| $P_\perp$        | 0                           |                             |
| $P_z$            | 0.7                         |                             |
| $\phi_e$         | $\pi/2$                     |                             |
|                  | horizontal plane (x)        | vertical plane (y)          |
| $\epsilon_{x,y}$ | $4.49 \times 10^{-9}$ m.rad | $4.5 \times 10^{-11}$ m.rad |
| $\beta_{x,y}$    | 96.46 m                     | 127.09 m                    |
| $\alpha_{x,y}$   | -8.72                       | 9.45                        |
| $\eta_{x,y}$     | -0.083 m                    | $-1.1 \times 10^{-9}$ m     |
| $\eta'_{x,y}$    | -0.0035                     | $6.8 \times 10^{-11}$       |

263 Compton scattering is then simulated using Eq. 2.2 by means of a Monte-Carlo accept-reject  
 264 method. The mean number of expected photons  $n_{\text{exp}} = \sigma_C \mathcal{L}$  per bunch crossing is estimated by

265 computing the total integrated cross-section for Compton scattering

$$\sigma_C = \frac{2\pi r_e^2}{x_c} \left( \left( 1 - \frac{4}{x_c} - \frac{8}{x_c^2} \right) \log(1+x_c) + \frac{1}{2} + \frac{8}{x_c} - \frac{1}{2(1+x_c)^2} \right) \quad (3.5)$$

$$+ P_C P_z \left( \left( 1 + \frac{2}{x_c} \right) \log(1+x_c) - \frac{5}{2} + \frac{1}{1+x_c} - \frac{1}{2(1+x_c)^2} \right) \quad (3.6)$$

266 and the luminosity of the interaction

$$\mathcal{L} = \frac{\lambda U Q_e}{2\pi h c q_e \sqrt{\sigma_{y,l}^2 + \sigma_{y,e}^2} \sqrt{\sigma_{x,l}^2 + \sigma_{x,e}^2 + \tan^2 \frac{\theta_{\min}}{2} (\sigma_{z,l}^2 + \sigma_{z,e}^2)}}, \quad (3.7)$$

267 where  $U$  denotes the laser pulse energy and  $q_e$  the elementary charge. For each simulated bunch  
 268 crossing the actual number of photons is taken according to a Poisson distribution with mean  
 269  $n_{\text{exp.}} \approx 0.06$  with the given nominal parameters. Random numbers  $\phi$  and  $y_c$  are generated using  
 270 uniform distributions in the range  $[0, 2\pi]$  and  $[y_{\min}, y_{\max}]$ , respectively, where

$$y_{\min} = x_c / (2\gamma^2 (1 - \cos \theta_{\max}) + x_c), \quad (3.8)$$

$$y_{\max} = x_c / (1 + x_c), \quad (3.9)$$

within approximations that are valid with a precision better than  $10^{-6}$ . The emission polar angle of  
 photons is computed as

$$\theta_\gamma = \arccos \left( \frac{1 - \frac{x_c(1-y_c)}{2\gamma^2 y_c}}{\beta} \right).$$

271 The transverse position of the photons at the entrance plane of the detector is then computed as

$$x_D = \delta_x + x_e + \tan(\delta_{x'} + x'_e) L + \cos \phi \tan \theta_\gamma L \quad (3.10)$$

$$y_D = \delta_y + y_e + \tan(\delta_{y'} + y'_e) L + \sin \phi \tan \theta_\gamma L, \quad (3.11)$$

272 where  $\delta_{x,y}$  and  $\delta_{x',y'}$  are inserted to account for spatial and angular misalignments, respectively.  
 273 Generated photons are then kept only if they fall inside the entrance plane of the photon detector.  
 274 This procedure allows to account for different geometries of the detector, as cylindrical or cuboid  
 275 shapes. Parameters related to the laser are summarized in Table 2.

276 Main identified backgrounds for the measurement of photon's energy are synchrotron radiation,  
 277 bremsstrahlung on the residual gas of the vacuum chamber and Compton radiation of electrons of  
 278 the beam on the photons from the black-body radiation in the vacuum chamber [14]. Synchrotron  
 279 radiation spectrum is estimated assuming that a 4 mm copper window is used in front of the photon  
 280 detector. The number of photons from synchrotron radiation passing through the window without  
 281 interaction is estimated using

$$N_{\text{th}} \approx \int_{E=E_{\min}}^{\infty} \frac{dN}{dE}(E) \exp(-t_{\text{Cu}} \rho_{\text{Cu}} / \lambda_{a,\text{Cu}}(E)) dE \quad (3.12)$$

$$\frac{dN}{dE}(E) = \sqrt{3} \alpha \frac{\theta_B}{2\pi} \frac{\gamma}{E_c} \int_{x=E/E_c}^{\infty} K_{5/3}(x) dx \quad (3.13)$$

**Table 2.** Table of nominal laser beam parameters used for the simulation.

| Parameter                    | Value   |
|------------------------------|---|
| $P_C$                        | -1  |
| $P_L$                        | 0   |
| $\phi_l$                     | 0   |
| $\sigma_x/\sigma_y/\sigma_z$ | 500 $\mu\text{m}/500 \mu\text{m}/500 \mu\text{m}$ |
| $\lambda$                    | 515 nm  |
| $f_{\text{rep.}}$            | 250 MHz   |
| $U$                          | 20 nJ   |
| $\theta_{in}$                | 8.9 degrees                                       |
| $\phi_{in}$                  | 28 degrees  |

where  $K_{5/3}(x)$  is a modified Bessel function of the second kind [37]. Data for absorption length in copper  $\lambda_{a,\text{Cu}}(E)$  for X-rays is taken from Ref. [40, 41]. The corresponding spectrum of the non-interacting photons is found to be roughly bell-shaped at about 60 keV with an RMS width of 10 keV approximately. The total energy deposited in the detector per bunch crossing due to synchrotron radiation is thus estimated to be about 3 keV for a 10 nC electron bunch. The related background will thus consist of a peaky distribution at very low energies with respect to that of photons originating from Compton scattering. It will correspond to a fluctuating energy pedestal that will negligibly contribute to the finite energy resolution of the measurements. A more accurate estimation is in order by means of detailed GEANT4 simulation since the window will effectively induce an electromagnetic shower that complicates this simple picture. At the conceptual design stage we decide to neglect this contribution in the simulation.

The bremsstrahlung of electrons on the residual gas in the beam pipe is approximated with the differential cross-section formula [42]

$$\frac{d\sigma_{\text{BG}}}{dy_c} = \frac{4\alpha r_e^2}{y_c} \left( \left( \frac{4(1-y_c)}{3} + y_c^2 \right) \left( Z^2 \log \left( \frac{184.15}{Z^{1/3}} \right) + Z \log \left( \frac{1194}{Z^{2/3}} \right) \right) + (1-y_c) \frac{Z+Z^2}{9} \right), \quad (3.14)$$

where  $Z \approx 2.5$  is the average atomic charge number of atoms contained in the residual gas. It is an empirical quantity that has been estimated for SuperKEKB in previous studies [25]. The expected number of photons from bremsstrahlung  $n_{\text{BG}} = \frac{Q_e}{q_e} \sigma_{\text{BG}} \frac{L_s P}{k_B T}$ , where  $L_s = 20$  m is the length of the straight section where the Compton interaction point is located,  $P = 5 \times 10^{-8}$  Pa the average residual gas pressure in the same region [25],  $T = 300$  K the temperature of the vacuum pipe and  $k_B$  the Boltzmann constant. The differential cross-section is analytically integrated in the range  $[E_{\text{cut-off}}, \mu_E]$  to provide

$$\sigma_{\text{BG}} = \frac{2Z\alpha r_e^2}{9} \left( -2 \log(\mathcal{E}) \left( 1 + Z + 12 \log \left( \frac{1194}{Z^{2/3}} \right) \right) - (1 - \mathcal{E}) \left( 2(1 + Z) + (15 - 9\mathcal{E}) \log \left( \frac{1194}{Z^{2/3}} \right) \right) - 3Z \left( 5 - 8\mathcal{E} + 3\mathcal{E}^2 + 8 \log(\mathcal{E}) \right) \log \left( \frac{184.15}{Z^{1/3}} \right) \right), \quad (3.15)$$

where  $\mathcal{E} = E_{\text{cut-off}}/\mu_E$ . The cut-off energy for observing a photon from bremsstrahlung is taken to be 1 MeV in the simulation. Changing the value of this cut-off affects the level of background at

304 low energies where the Compton spectrum is not sensitive to the polarization of the electron beam.  
 305 This threshold is chosen fixed in the present study but may be modified in the next stages of the  
 306 development of the detector. The actual number of photons from bremsstrahlung per simulated  
 307 bunch crossing is taken randomly following a Poisson distribution.

308 Electrons also experience Compton scattering on the thermal photons that are in the vacuum  
 309 pipe of the accelerator. In order to estimate the number of scattered photons, the convolution of the  
 310 thermal photon density and the Compton cross-section is computed as [43]

$$\frac{dN_{\text{BB}}}{dy_c} = \frac{Q_e L_s}{2\pi^2 q_e c^3 \hbar^3} \int_{\theta_0=0}^{\pi} \int_{\omega=\omega_0}^{\infty} \frac{d\sigma}{dy_c}(\theta_0, \omega) \frac{\omega^2 (1 + \cos(\theta_0))}{e^{(\omega/(k_B T))} - 1} d\omega d \cos(\theta_0), \quad (3.16)$$

$$\omega_0 = \frac{m_e^2 c^4 y_c}{2(1 + \cos(\theta_0))(1 - y_c)\mu_E}, \quad (3.17)$$

311 where  $\pi - \theta_0$  denotes the angle made by thermal photons of energy  $\omega$  with electrons of the beam.  
 312 Similarly as for synchrotron radiation, the thickness of the copper window in front of the detector  
 313 cuts-off the lower energy part of the spectrum. The number of black-body photons is thus estimated  
 314 in a similar fashion as in Eq. 3.12 to be about 0.04 in average per bunch crossing corresponding to a  
 315 700 keV average deposited energy. These may seem small but the corresponding spectrum extends  
 316 towards relatively large energies, around up to 100 MeV, see Fig. 5. It would thus contribute to  
 317 the very first bins in the measured photon energy histograms where there is no sensitivity to the  
 318 polarization. These bins are ignored, see following text, in the fit and the contribution from thermal  
 319 photons is not included in the simulation.

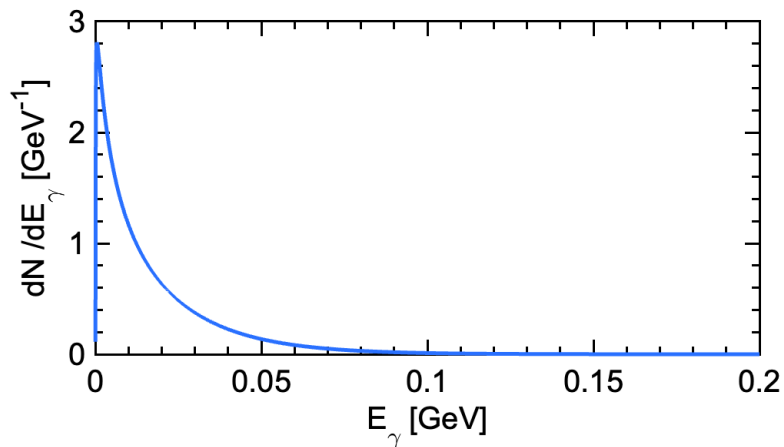


**Figure 5.** Spectrum of photons emitted from the interaction of electrons with thermal photons emitted by the black-body radiation related to the finite temperature of the vacuum pipe.

320 For Compton and background processes, photons are generated and their energies are summed  
 321 up for every simulated bunch crossing, provided that they are impinging the detector. The small  
 322 angle of the photon's direction with the normal of the detector entrance plane, a square with 5 mm  
 323 sides located 13 m downstream the Compton interaction point, is neglected and the electromagnetic  
 324 shower is assumed to be fully contained in the detector. The effect of the transverse and longitudinal  
 325 extensions of the electromagnetic shower is neither simulated at this stage. These crude assumptions

326 will be removed at a later stage of the design of the detector. In a first approximation it will induce  
 327 an overall calibration factor and a degradation of the detector resolution. It will also likely induce a  
 328 residual energy dependence of the calibration factor, the scale of which being assumed negligible  
 329 at this stage, but will be carefully evaluated based on detector prototyping and further detailed  
 330 simulations. At this stage of the study the total deposited energy is randomly smeared according to  
 331 a normal distribution centered on the expected total incident energy  $E_{\text{in}}$  and with a width

$$\sigma_{E_{\text{in}}} = E_{\text{in}} \sqrt{\frac{A_{\text{det.}}^2}{E_{\text{in}}^2} + B_{\text{det.}}^2}. \quad (3.18)$$

332 Parameters related to the detector are summarized in Table 3. Accounting for conversion efficiency  
 333 of photons' energy to fluorescence of 0.1, quantum efficiency of 0.1 and light collection efficiency of  
 334 the photomultiplier of 0.1, one expects to collect about 1800 photo-electrons at 1 GeV which would  
 335 induce a few percent energy resolution assuming that it is dominated by the contribution related to  
 336 the PMT. At this stage we will rather assume for the simulations a 10 % resolution related to the  
 337 stochastic term due to remaining uncertainties at this stage of the design. A constant term of 1 % is  
 338 also added. Attention will be paid to this contribution during the development of the detector, since  
 339 one main source is related to pedestal fluctuation that may be large due to a possibly significant  
 340 pile-up related to the small time separation of the incoming photons of about 4 ns. The obtained  
 341 smeared energy is then stored in a histogram that will be further analyzed to extract the polarization  
 342 parameters. Measurements of the polarization of every bunch is expected to last approximately the  
 343 time in between two refreshments of electron bunches i.e. a few minutes. We will assume that  
 344 measurements are nominally done over  $T_{\text{meas.}} = 5 \text{ min}$  which corresponds to  $T_{\text{meas.}}/T_{\text{rev.}} = 30 \times 10^6$   
 bunch crossings per bunch.

**Table 3.** Table of nominal parameters used to simulate the Compton interaction and the detector.

| Parameter          | Value                   |
|--------------------|-------------------------|
| $L$                | 13 m                    |
| $T_{\text{meas.}}$ | 5 min                   |
| $d_{\text{det.}}$  | 5 cm                    |
| $A_{\text{det.}}$  | $0.1 \text{ GeV}^{1/2}$ |
| $B_{\text{det.}}$  | 0.01                    |

345

### 346 3.2 Fitting procedure

347 Fit of the generated data with the known theoretical expressions of the differential cross-sections  
 348 provides sensitivity to the a priori unknown parameters, including the electron beam polarization.  
 349 The model used for the bremsstrahlung background contribution is only an approximation, and the  
 350 experimental results may differ to some extent. Thus regular dedicated background measurement  
 351 runs may be considered by switching off the laser and measuring the background only, dominated  
 352 by the bremsstrahlung. Periodicity of such background measurements will be determined by a study  
 353 of the reproducibility and drifts in this distribution with time. It is expected to provide an empirical  
 354 distribution for the background that is further used for the fit of data taken with the laser switched

355 on. Signal is described by the Eq. 2.1 integrated over the non-observed angle  $\phi$  providing

$$\frac{d\sigma}{dy_c} = \frac{d\sigma_0}{dy_c} + P_C P_z \frac{d\sigma_1}{dy_c}. \quad (3.19)$$

356 Two terms are distinguished one independent of  $P_C$  and another proportional to  $P_C$ . Since events  
357 with two Compton photons may be observed, the three convolution terms are needed

$$\frac{d\sigma_{ij}}{dy_c}(y_c) = \int_{\max(y_{\min}, y_c - y_{\max})}^{\min(y_{\max}, y_c - y_{\min})} \frac{d\sigma_i}{dy_c}(y_0) \frac{d\sigma_j}{dy_c}(y_c - y_0) dy_0. \quad (3.20)$$

358 The contributions corresponding to four Compton photons or more are neglected at this stage of  
359 the development. They are found small compared to statistical fluctuations of other contributions  
360 including the background level in the high-energy end of the spectrum. We are thus left with nine,  
361 signal related contributions that are stored in look up tables (LUTs). Similarly the contributions with  
362 one bremsstrahlung photon and its convolution with one or two Compton photons are computed. It  
363 makes six additional terms. These 15 contributions are each convoluted with the energy resolution  
364 function used to generate the events and the results stored in LUTs. They are then used to fill-in  
365 new LUTs with the exact size of the histograms that were filled in at generation level accounting for  
366 a possible miscalibration scale that can be fit by the algorithm without the need to compute again  
367 all previous convolutions. These 15 histograms are then summed up with five free parameters:  
368 three scale factors for the yield of one, two and three Compton photons; a scale factor for the  
369 bremsstrahlung contribution; the longitudinal polarization of the electron beam. The contributions  
370 corresponding to convolution of bremsstrahlung and Compton photons are scaled using the same  
371 scale factors as for the signal, to avoid a large number of free scale factors corresponding to very  
372 small number of events. A  $\chi^2$  is built using the expected number of events in each bin and the  
373 Monte Carlo data. It is normalized using the statistical uncertainty of the data. Bins corresponding  
374 to photon's energies below 200 MeV are discarded from the  $\chi^2$  calculation. This makes the fit robust  
375 against a possible mis-control of the background distribution below 200 MeV. A typical fit result  
376 is shown on Fig. 6, where the generated Monte Carlo events are shown along with the fit result,  
377 explicitly showing each contribution. We note that the fit is excellent spanning over five orders of  
378 magnitude, thanks to the different characteristic energy end points of Compton and Bremsstrahlung  
379 photons.

380 This procedure allows to have a very fast fit, that permits to treat the 2500 stored histograms in  
381 approximately a minute on a modern commercial laptop, i.e. well before a new set of acquisitions is  
382 available. It provides an on-line measurement of the polarization. Storage of histograms would be  
383 done to permit further offline analysis of the data in case it is needed. This procedure assumes that  
384 most parameters are constant except fractions for each species and the beam polarization. Indeed  
385 the detector response, as calibration and energy resolution, is not expected to vary quickly. Regular  
386 offline calibration can be planned from time to time by performing a fit with the corresponding  
387 parameters free to vary. This has been validated by with a dedicated toy Monte Carlo study.  
388 Background spectrum can also be regularly calibrated by taking regular laser-off acquisitions. The  
389 acquisition system and the laser control must be able to cope with the necessary flexibility. A  
390 similar procedure was employed in the past [14].

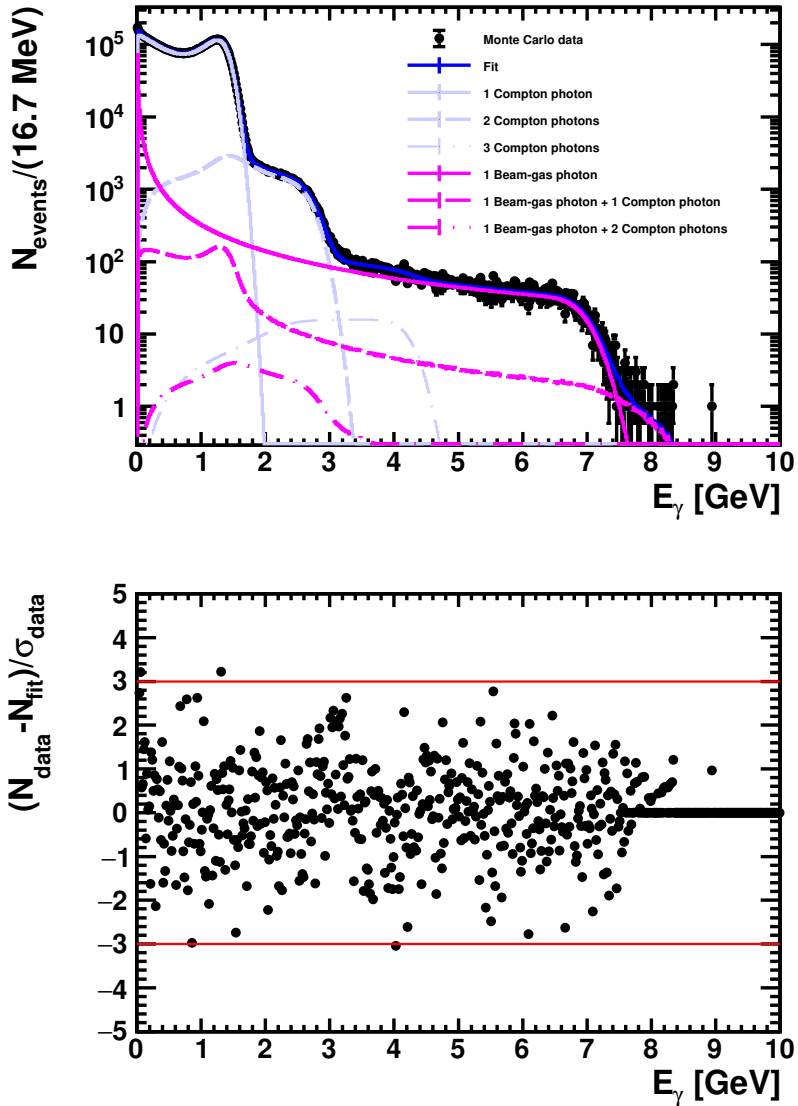


**Figure 6.** (Top) a typical example of a Monte Carlo experiment representing 25 min of data taking in the polarimeter. Black dots with error bars represent the Monte-Carlo data, the blue (dark grey line superimposed to the data) line is the fit result that is the sum of the contributions related to Compton scattering in light blue or light-grey (one-photon in plain line, two-photons in dashed line, three-photons in dash-dotted line) and those related to Bremsstrahlung in magenta or grey (one Bremsstrahlung photon in plain line, one Bremsstrahlung photon and one Compton photon in dashed line, one Bremsstrahlung photon and two Compton photons in dash-dotted line). (Bottom) residuals of the fit normalized by the statistical uncertainty in the simulated data. The red (grey) lines materialize three standard deviations between the fit and the simulated data.

### 391 3.3 Results

392 A toy Monte Carlo procedure is applied to validate the fitting procedure and assess preliminary  
393 systematic uncertainties. First a signal only study is performed to assess the accuracy of the fast  
394 fitting procedure. The statistical precision for a single bunch is estimated by generating events  
395 corresponding to several data-taking duration  $t_{dt}$  ranging from one to 25 minutes and shown on  
396 Figure 7. For that purpose a thousand toy Monte-Carlo experiments are thrown for each value of  
397  $t_{dt}$ . The statistical accuracy for each bunch over  $t_{dt} = 5$  min is about 1%, a duration similar to two  
398 successive refreshing of the given bunch population. Beside the statistical precision, the robustness  
399 of the fit model is tested assuming that  $t_{dt} = 25$  min, which allows to obtain a more accurate  
400 estimate of possibly biasing effects. We test the accuracy of the fit model by fitting not only signal  
401 but also letting a global calibration scale and the stochastic term of the detector resolution free.  
402 These parameters are fit together with fraction of events and the beam polarization with a relative  
403 precision of  $10^{-4}$  and  $10^{-3}$  respectively, without significant bias. The polarization parameter  $P_z$   
404 however exhibits a small but significant bias of  $8 \times 10^{-4}$  in the signal only fit procedure. It is observed  
405 that when the stochastic term of the detector resolution is improved from  $0.1 \text{ GeV}^{1/2}$  to  $0.03 \text{ GeV}^{1/2}$ ,  
406 this bias disappears. At this stage it is difficult to ensure that a resolution better than  $0.1 \text{ GeV}^{1/2}$   
407 will be obtained, and thus we assign a systematic uncertainty of 0.08% to the extraction of the  
408 polarization that we dub *fit model*. No observable bias is observed when generating events with a  
409 nuisance linear laser polarization of  $P_L = 0.05$ , assuming that the degree of circular polarization  
410 of the laser is  $P_C = \sqrt{1 - P_L^2} \approx 1 - 0.0013$ . However the knowledge of the degree of circular  
411 polarization of the laser may be imperfect, as it was found in previous experiments. We assign a  
412 0.3% systematic uncertainty, though recently a factor three better performance was demonstrated  
413 [19]. A similar procedure is applied for a nuisance transverse electron beam polarization that is not  
414 expected to affect the measured spectrum of photons due to the integration performed by the detector  
415 in the transverse plane. Again, no bias is observed within the statistical accuracy of the toy Monte  
416 Carlo procedure. We thus assign, as a systematic uncertainty 0.015% for both of these effects.  
417 This value corresponds to the standard deviation on the determination of the average bias, that is  
418 compatible with zero. The fit procedure assumes a known energy of the electron beam, despite  
419 that beam energy spread is accounted for in the generation of the events. Unfortunately, fitting this  
420 parameter along with an overall calibration scale and the energy resolution of the detector shows  
421 strong correlations that prevent the fit to provide useful information on the actual beam energy.  
422 We test the impact of a mis-knowledge of the beam energy by shifting it by  $10 \mu_E \sigma_\delta \approx 44 \text{ MeV}$   
423 which represents a change in energy that is larger than changes of energy observed with the Belle  
424 II detector [44]. A bias of 0.05% is observed and added as a systematic uncertainty. Furthermore,  
425 the effect of a 2 mm spatial and 100  $\mu\text{rad}$  angular misalignments have been tested and not found to  
426 induce a bias, and thus we accordingly assign a systematic uncertainty of 0.015% for both of these.  
427 A longitudinal misalignment, corresponding to a shift of the Compton interaction point and/or the  
428 detector along the beam direction of 1 cm has been implemented in the simulation and not found to  
429 induce a bias either. It would indeed modify slightly the size of the photon beam on the detector.  
430 A systematic uncertainty of 0.015% is thus assigned to this possible effect. Since SuperKEKB is  
431 using a betatron injection scheme, the center of mass of each freshly injected bunch is shaken and  
432 the emittance grows and returns to equilibrium in several thousands of turns. This effect has been

433 simulated and not found to affect the performance of the polarimeter. Indeed the induced transverse  
 434 oscillations are small with respect to the previously tested misalignments, and the effect thus limits  
 435 to an effective reduction of luminosity, that does not affect the performance of the polarimeter. No  
 436 systematic uncertainty is thus assigned for this.

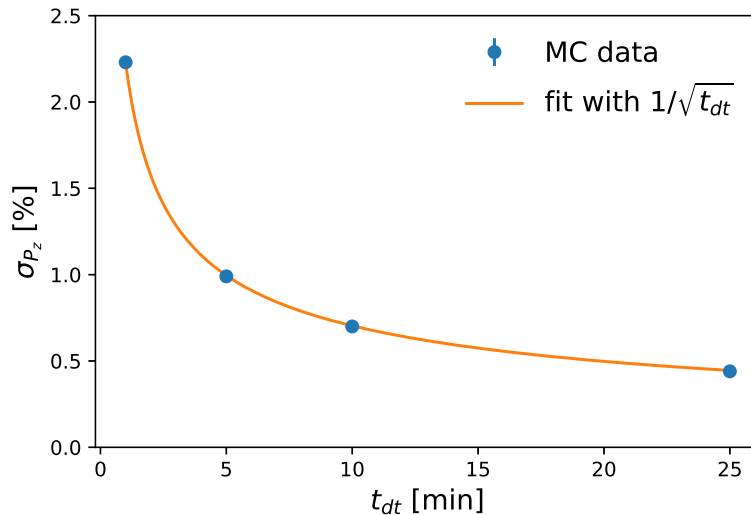


**Figure 7.** Statistical precision of the Compton polarimeter as a function of the duration of the data taking  $t_{dt}$  for a single bunch. For 25 minutes of data taking, a 0.5% statistical precision is obtained. Monte Carlo uncertainties on the points are negligible and smaller than the size of the points. The orange curve is a  $1/\sqrt{t_{dt}}$  fit of the points, showing that the statistical precision behaves as expected.

437 A final residual systematic uncertainty lies in the knowledge of the background model. To test  
 438 this hypothesis, a fit of the background model is first performed to estimate the accuracy with which  
 439 one is able to extract its model parameter  $Z$ . This is done by means of a toy Monte-Carlo and yields  
 440 to  $Z = 2.47 \pm 0.07$  for a generated  $Z_{\text{gen.}} = 2.50$ . In practice, since the model employed here is only  
 441 an approximation, a careful study is in order to either validate the model or directly feed laser-off  
 442 measured distributions in the fit of laser-on data. It is currently planned to perform this study  
 443 during dedicated beam test experiments before the implementation of the Compton polarimeter,  
 444 and thus remains out of the scope of this paper. In order to give an insight on the sensitivity of the  
 445 fit to the background model we thus generate the background by randomly varying the parameter  
 446  $Z$  with a Gaussian distribution centered on  $Z = 2.50$  and with a width of  $\sigma_Z = 0.07$ , for each  
 447 toy Monte-Carlo experiment, and keep  $Z = 2.50$  fixed in the fit. A bias of 0.16% is obtained,  
 448 that we assign as a systematic uncertainty. An overall systematic uncertainty of 0.35% is obtained  
 449 comparable to the statistical uncertainty reached over 25 minutes, and the sources are summarized  
 450 in Table 4.

451 It must be noted that a detailed detector simulation and performance validation on a prototype  
 452 detector is planned in order to confirm the systematic uncertainties assigned at this conceptual  
 453 stage of the design of the polarimeter. It will also allow to understand the actual energy resolution  
 454 and non linearity in the energy scale. Furthermore beam-based experiments are also needed to

**Table 4.** Systematic uncertainties on the extraction of  $P_z$ , see text for details. Background modeling and absolute knowledge of the laser polarization dominates.

| Source                                | Uncertainty on $P_z$ (%) |
|---------------------------------------|--------------------------|
| Laser beam polarization               | 0.30                     |
| Backgrounds                           | 0.16                     |
| Fit procedure                         | 0.080                    |
| Beam energy                           | 0.050                    |
| Spatial misalignment                  | 0.015                    |
| Angular misalignment                  | 0.015                    |
| Longitudinal misalignment             | 0.015                    |
| Transverse electron beam polarization | 0.015                    |
| Total                                 | 0.35                     |

455 validate the background model with SuperKEKB data at the expected location of the polarimeter to  
456 understand its actual influence on the detector performance, since it is one of the dominant systematic  
457 uncertainties. Finally the measurement of the longitudinal polarization of the electron at the location  
458 of the polarimeter remains to be converted to a figure at the Belle II interaction point. Fortunately the  
459 expected polarization at the Belle II interaction point is identical to that at the Compton polarimeter,  
460 and thus it provides a meaningful measurement. However systematic uncertainties in the spin  
461 transport remain to be evaluated in order to compare the Compton polarimeter measurement with  
462 a direct measurement of the electron beam polarization by use of  $e^+e^- \rightarrow \tau^+\tau^-$  data [45].

## 463 4 Summary

464 We have proposed a concept of a Compton polarimeter able to cope with the high repetition rate  
465 of the SuperKEKB ring. Integration of this polarimeter in the existing SuperKEKB lattice is found  
466 possible and the necessary modifications are not found to affect the electron beam dynamics of this  
467 high-luminosity collider. The proposed laser system will be directly integrated in the accelerator  
468 which is not found to be an issue with respect to the level of radiation in the accelerator. A concept  
469 of photon detector is proposed to diagnose the scattered photons and a first assessment of systematic  
470 uncertainties show that they amount to about 0.4%. Similar statistical uncertainty will be reached  
471 for every bunch every 25 minutes. The proposed extraction procedure for the polarization is found  
472 to allow on-line measurements of every bunch with a 1% precision on time-scales corresponding  
473 to single bunch top-up in the accelerator. Further work is now considered to realize a prototype  
474 of the photon detector to be integrated in the SuperKEKB accelerator and validate the background  
475 model with experimental data. Overall, this study paves the way to wards implementing real-time  
476 polarimetry at SuperKEKB and other future projects, as EIC for instance.

## 477 Acknowledgments

478 We thank the Belle II, SuperKEKB and polarization upgrade project collaborators, in particular  
479 Shuji Tanaka, John Michael Roney for fruitful discussions. IJCLab members also thank Giulia Hull

480 and Bernard Genolini for useful discussions.

## 481 **References**

- 482 [1] E Kou et al. The Belle II Physics Book. *Progress of Theoretical and Experimental Physics*, 2019(12),  
483 December 2019. [\\_eprint:  
484 https://academic.oup.com/ptep/article-pdf/2019/12/123C01/32693980/ptz106.pdf.](https://academic.oup.com/ptep/article-pdf/2019/12/123C01/32693980/ptz106.pdf)
- 485 [2] Demin Zhou, Kazuhito Ohmi, Yoshihiro Funakoshi, Yukiyoishi Ohnishi, and Yuan Zhang.  
486 Simulations and experimental results of beam-beam effects in superkekb. *Phys. Rev. Accel. Beams*,  
487 26:071001, Jul 2023.
- 488 [3] Y. Funakoshi et al. The SuperKEKB Has Broken the World Record of the Luminosity. In *Proc. 13th*  
489 *International Particle Accelerator Conference (IPAC'22)*, number 13 in International Particle  
490 Accelerator Conference, pages 1–5. JACoW Publishing, Geneva, Switzerland, 07 2022.
- 491 [4] M. Gabriel et al. A time resolved study of injection backgrounds during the first commissioning phase  
492 of SuperKEKB. *The European Physical Journal C*, 81(11):972, November 2021.
- 493 [5] Francesco Forti. Snowmass whitepaper: The belle ii detector upgrade program, 2022.
- 494 [6] A. Accardi et al. Snowmass 2021 white paper on upgrading superkekb with a polarized electron  
495 beam: Discovery potential and proposed implementation, 2022.
- 496 [7] Jose Bernabeu, Gabriel A. González-Sprinberg, Joannis Papavassiliou, and Jordi Vidal. Tau  
497 anomalous magnetic moment form factor at super b/flavor factories. *Nuclear Physics*, 790:160–174,  
498 2007.
- 499 [8] Caleb Miller. Measurement of beam polarization at an  $e^+e^-$  b-factory with new tau polarimetry  
500 technique, 2022.
- 501 [9] D.B. Gustavson et al. A backscattered laser polarimeter  $e^+e^-$  storage rings. *Nuclear Instruments and*  
502 *Methods*, 165(2):177–186, 1979.
- 503 [10] H. D. Bremer, H. C. Dehne, H. C. Lewin, H. Mais, R. Neumann, R. Rossmanith, and R. Schmidt. The  
504 petra-polarimeter. In C. Joseph and J. Soffer, editors, *High-Energy Physics with Polarized Beams and*  
505 *Polarized Targets*, pages 469–471, Basel, 1981. Birkhäuser Basel.
- 506 [11] D.P. Barber et al. A precision measurement of the  $\nu'$  meson mass. *Physics Letters B*, 135(5):498–504,  
507 1984.
- 508 [12] L. Knudsen, J.P. Koutchouk, M. Placidi, R. Schmidt, M. Crozon, J. Badier, A. Blondel, and  
509 B. Dehning. First observation of transverse beam polarization in lep. *Physics Letters B*,  
510 270(1):97–104, 1991.
- 511 [13] D.P. Barber et al. The hera polarimeter and the first observation of electron spin polarization at hera.  
512 *Nuclear Instruments and Methods in Physics Research Section A: Accelerators, Spectrometers,*  
513 *Detectors and Associated Equipment*, 329(1):79–111, 1993.
- 514 [14] S Baudrand, M Bouchel, V Brisson, R Chiche, M Jacquet, S Kurbasov, G Li, C Pascaud, A Reboux,  
515 V Soskov, Z Zhang, F Zomer, M Beckingham, T Behnke, N Coppola, N Meyners, D Pitzl, S Schmitt,  
516 M Authier, P Deck-Betinelli, Y Queinec, and L Pinard. A high precision fabry-perot cavity  
517 polarimeter at hera. *Journal of Instrumentation*, 5(06):P06005, jun 2010.
- 518 [15] V.E. Blinov, T.V. Bedareva, S.A. Zakharov, V.V. Kaminskiy, V.N. Kudryavtsev, N.Yu. Muchnoi, S.A.  
519 Nikitin, I.B. Nikolaev, and L.I. Shekhtman. Status of laser polarimeter at vepp-4m. *Journal of*  
520 *Instrumentation*, 15(08):C08024, aug 2020.

- 521 [16] I. Passchier, D. W. Higinbotham, C. W. de Jager, B. E. Norum, N. H. Papadakis, and N. P. Vodinas. A  
522 Compton backscattering polarimeter for measuring longitudinal electron polarization, 1999.
- 523 [17] M Beckmann, A Borissov, S Brauksiepe, F Burkart, H Fischer, J Franz, F.H Heinsius, K Königsmann,  
524 W Lorenzon, F.M Menden, A Most, S Rudnitsky, C Schill, J Seibert, and A Simon. The longitudinal  
525 polarimeter at HERA. *Nuclear Instruments and Methods in Physics Research Section A: Accelerators,  
526 Spectrometers, Detectors and Associated Equipment*, 479(2):334–348, 2002.
- 527 [18] S. Escoffier et al. Accurate measurement of the electron beam polarization in JLAB Hall A using  
528 Compton polarimetry. *Nuclear Instruments and Methods in Physics Research Section A: Accelerators,  
529 Spectrometers, Detectors and Associated Equipment*, 551(2):563–574, 2005.
- 530 [19] A. Narayan et al. Precision electron-beam polarimetry at 1 GeV using diamond microstrip detectors.  
531 *Phys. Rev. X*, 6:011013, Feb 2016.
- 532 [20] Christoph Bartels, Anthony Hartin, Christian Helebrant, Daniela Käfer, and Jenny List. Precision  
533 polarimetry at the ILC: Concepts, simulations and experiments. *Nuclear Instruments and Methods in  
534 Physics Research Section A: Accelerators, Spectrometers, Detectors and Associated Equipment*,  
535 623(1):570–572, 2010. 1st International Conference on Technology and Instrumentation in Particle  
536 Physics.
- 537 [21] S.H. Chen et al. A toy Monte Carlo simulation for the transverse polarization of high-energy electron  
538 beams. *Journal of Instrumentation*, 17(08):P08005, Aug 2022.
- 539 [22] Ferdinand Willeke and J. Beebe-Wang. Electron ion collider conceptual design report 2021, 2 2021.
- 540 [23] N.Yu. Muchnoi. Electron beam polarimeter and energy spectrometer. *Journal of Instrumentation*,  
541 17(10):P10014, Oct 2022.
- 542 [24] Y. Suetsugu, K. Shibata, T. Ishibashi, M. Shirai, S. Terui, K. Kanazawa, H. Hisamatsu, and M. L. Yao.  
543 SuperKEKB vacuum system operation in the last 6 years operation. *Phys. Rev. Accel. Beams*,  
544 26:013201, Jan 2023.
- 545 [25] Z. Liptak et al. Measurements of beam backgrounds in SuperKEKB phase 2. *Nuclear Instruments and  
546 Methods in Physics Research Section A: Accelerators, Spectrometers, Detectors and Associated  
547 Equipment*, 1040:167168, 2022.
- 548 [26] O. Klein and Y. Nishina. Über die Streuung von Strahlung durch freie Elektronen nach der neuen  
549 relativistischen Quantendynamik von Dirac. *Zeitschrift für Physik*, 52(11):853–868, November 1929.
- 550 [27] I.F. Ginzburg, G.L. Kotkin, S.L. Panfil, V.G. Serbo, and V.I. Telnov. Colliding  $\gamma e$  and  $\gamma\gamma$  beams  
551 based on single-pass  $e^+e^-$  accelerators II. Polarization effects, monochromatization improvement.  
552 *Nuclear Instruments and Methods in Physics Research*, 219(1):5–24, 1984.
- 553 [28] Gilles Buchs, Stefan Kundermann, Erwin Portuondo-Campa, and Steve Lecomte. Radiation hard  
554 mode-locked laser suitable as a spaceborne frequency comb. *Opt. Express*, 23(8):9890–9900, Apr  
555 2015.
- 556 [29] Yoon-Soo Jang, Joohyung Lee, Seungman Kim, Keunwoo Lee, Seongheum Han, Young-Jin Kim, and  
557 Seung-Woo Kim. Space radiation test of saturable absorber for femtosecond laser. *Opt. Lett.*,  
558 39(10):2831–2834, May 2014.
- 559 [30] S. Girard, A. Laurent, E. Pinsard, T. Robin, B. Cadier, M. Boutillier, C. Marcandella, A. Boukenter,  
560 and Y. Ouerdane. Radiation-hard erbium optical fiber and fiber amplifier for both low- and high-dose  
561 space missions. *Opt. Lett.*, 39(9):2541–2544, May 2014.
- 562 [31] M. Woods and representing the SLD collaboration. The scanning Compton polarimeter for the SLD  
563 experiment, 1996.

- 564 [32] U. Keller. Ultrafast solid-state laser oscillators: a success story for the last 20 years with no end in  
565 sight. *Applied Physics B*, 100(1):15–28, July 2010.
- 566 [33] Michalis N. Zervas. High power ytterbium-doped fiber lasers — fundamentals and applications.  
567 *International Journal of Modern Physics B*, 28(12):1442009, 2014.
- 568 [34] N. Vansteenkiste, P. Vignolo, and A. Aspect. Optical reversibility theorems for polarization:  
569 application to remote control of polarization. *J. Opt. Soc. Am. A*, 10(10):2240–2245, Oct 1993.
- 570 [35] Ren-Yuan Zhu. Ultrafast and radiation hard inorganic scintillators for future hep experiments. *Journal*  
571 *of Physics: Conference Series*, 1162(1):012022, jan 2019.
- 572 [36] R. L. Workman et al. Review of Particle Physics. *PTEP*, 2022:083C01, 2022.
- 573 [37] John David Jackson. *Classical electrodynamics*. Wiley, New York, NY, 3rd ed. edition, 1999.
- 574 [38] P. Chen, G. Horton-Smith, T. Ohgaki, A. W. Weidemann, and K. Yokoya. CAIN: Conglomerat  
575 d’ABEL et d’interactions nonlineaires. *Nucl. Instrum. Meth. A*, 355:107–110, 1995.
- 576 [39] K. Yokoya. CAIN:user manual.
- 577 [40] Stephen M. Seltzer. Calculation of photon mass energy-transfer and mass energy-absorption  
578 coefficients. *Radiation Research*, 136(2):147–170, 1993.
- 579 [41] NIST. X-ray mass attenuation coefficients.
- 580 [42] Yung-Su Tsai. Pair production and bremsstrahlung of charged leptons. *Rev. Mod. Phys.*, 46:815–851,  
581 Oct 1974.
- 582 [43] V.I. Telnov. Scattering of electrons on thermal radiation photons in electron-positron storage rings.  
583 *Nuclear Instruments and Methods in Physics Research Section A: Accelerators, Spectrometers,*  
584 *Detectors and Associated Equipment*, 260(2):304–308, 1987.
- 585 [44] Belle II Collaboration et al. Measurement of the  $\tau$ -lepton mass with the belle ii experiment, 2023.
- 586 [45] Caleb Miller. Measurement of Beam Polarization at an  $e^+e^-$  B-Factory with New Tau Polarimetry  
587 Technique. In *20th Conference on Flavor Physics and CP Violation*, 7 2022.